

metal electronic transport.

This work. While the predictions for phenomenology may capture aspects of the strange metal phase, the specific form of models like (1) is challenging to motivate: First, the Hamiltonian (1) lacks the notion of space, which in more realistic models is imposed by the locality of physical interactions. Second, the interaction in (1) is particle-number conserving, but not, in general, of the density-density type. The consequences of this latter observation we explore in this paper. Specifically, we study the model Hamiltonian

$$\hat{H}_{tU} = \sum_{ij}^{N_B} t_{ij} c_i^\dagger c_j + \sum_{ij}^{N_B} U_{ij} \hat{n}_i \hat{n}_j, \quad (2)$$

where $\hat{n}_i = c_i^\dagger c_i$. In contrast to Eq. (1), the model (2) has the attractive feature that its interaction term commutes with the local density \hat{n}_i and thus shares a fundamental symmetry with physical interactions, in particular, the Coulomb interaction. Other than this symmetry, we keep the model structureless as before with SYK: the constituting matrices t_{ij} and U_{ij} are taken to be a zero-mean complex Gaussian random number with variance $\langle t_{ij}^2 \rangle = t^2 / (64N_B)$ and $\langle U_{ij}^2 \rangle = U^2 / (64N_B)$; hermiticity requires $t_{ij} = t_{ji}^*$ and $U_{ij} = U_{ji} = U_{ij}^*$. As usual, the scale factor in the denominator ensures a volume-scaling of the total energy when taking the thermodynamic limit, see appendix A.

The properties of the model (2) will be explored in the following. We give a brief account of our findings. In Eq. (2) each term by itself is integrable in a many-body sense: While the bare interaction term conserves the local occupations, the kinetic term proper conserves the occupations of single-particle eigenstates. Due to this trivial integrability one finds two fixed points, each with Poisson-type level spacing at $t=0$ and $U=0$, respectively. These fixed-points, - which presumably become unstable already when t and U differ from zero, - are separated by a region exhibiting a Wigner-Dyson-type level statistics, see Fig. 1, with several subphases. The properties of these phases we characterize in terms of the inverse participation ratio in Fock-space and the spectral form factor. While the three sectors I, II/III, IV are naturally identified with phases found earlier by Micklitz *et al.* [30] and Monteiro *et al.* [31], the sector IV' differs from IV and has not been described before.

Finally, we calculate the imaginary frequency Green's function and compare it with the well-known conformal SYK results in the infrared and large N_B -limit: the frequency scaling of (2) is consistent with an SYK-type behavior. While the available system sizes are too small to make definite predictions for the thermodynamic limit, our results still suggest that both phases are adiabatically connected and therefore should be identified with each other. In this sense and similar to Ref. [16] our work tightens the link between the SYK-model and more realistic microscopic ones.

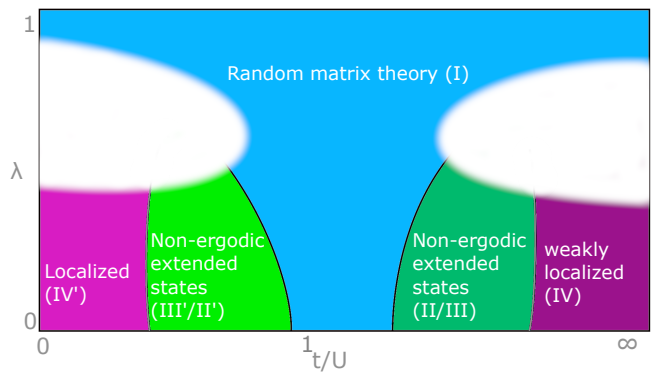


FIG. 1. Phase diagram of model Eq. (2). The parameter λ , defined in Eq. (6), interpolates between the complex SYK model (1), $\lambda=1$, and (2), $\lambda=0$. The regions I, II/III and IV have been identified according to the classification given in Ref. [31] Black phase boundaries denote phase transitions, while grey boundaries are expected to collapse with the left and right edges in the thermodynamic limit. Blank regions are unknown.

II. METHOD

In order to calculate statistical and dynamical properties we diagonalize Hamiltonian (2) exactly for a finite number of fermionic sites $N_B = 12, 16, 20$. [32] The Hamiltonian is written in Fock space in the occupation number basis of the operators \hat{n}_i . Recalling particle number conservation, the Hamiltonian matrix can be brought to block diagonal form, such that the effective Fock space dimension reduces considerably for the individual blocks associated with a specific filling. In this work we always choose a quarter filling. [33]

III. COMPUTATIONAL RESULTS

The close and prominent relation between the SYK model and random matrix theory (RMT) plays a crucial role for the holographic duality to black holes in two-dimensional gravity. [1] We therefore begin the outline of our computational results with the level spacing statistics $P(s)$, which is a hallmark of RMT-related physics. A subsequent analysis of level spacing ratios serves for a first mapping of the different phases involved and their respective boundaries. As it turns out, $P(s)$ and the level spacing ratios are blind to a subspace structure, which however readily emerges after consulting the spectral form factor $K(T)$. In fact, the form factor also can discriminate the localized phases IV and IV' from each other. The substructure of the delocalized phases also reveals in the inverse participation ratio, which we investigate subsequently. We conclude with a study of the frequency dependency of the Green's function.

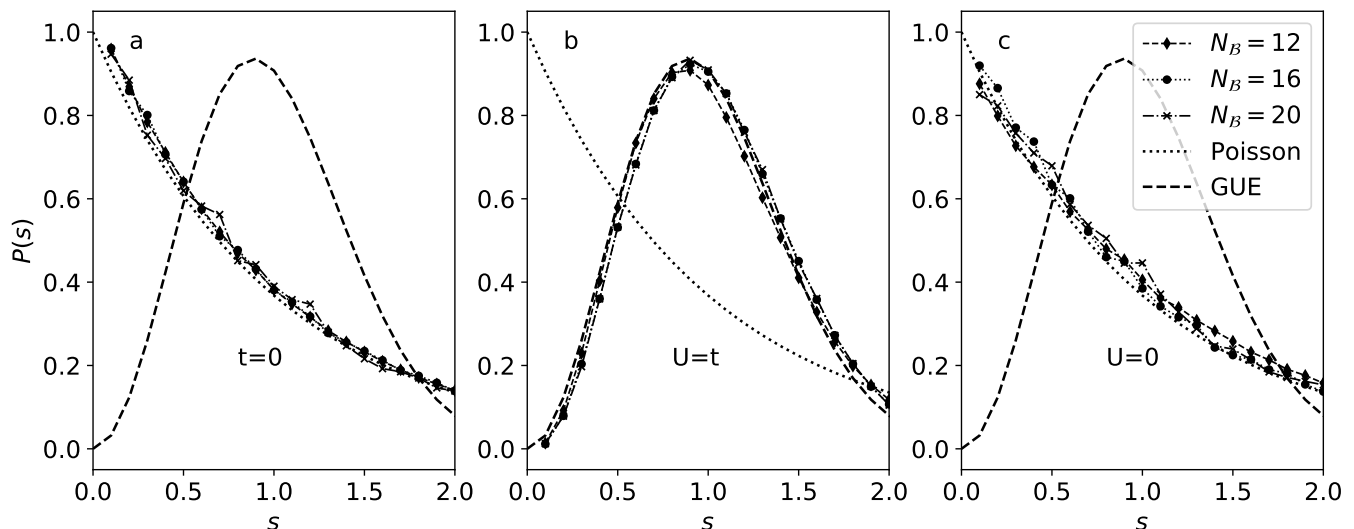


FIG. 2. Level spacing statistics in phases IV' (a), I (b), and IV (c); nomenclature defined in Fig. 1. Dashed curve indicates GUE prediction, dotted line the Poisson limit. (number of disorder realizations: 5000 for $N_B = 12$, 200 for $N_B = 16$ and 20 for $N_B = 20$. The filling is $1/4$.) The plot shows that despite the limited system sizes an assignment of localized vs delocalized to the respective phases is justified.

A. Level spacing statistics

Distribution function $P(s)$. The level-spacing distribution function is defined as

$$P(s) = \overline{\delta(s - s_l)}, \quad (3)$$

where $s_l = (E_l - E_{l-1})/\Delta$ denotes the spacing between two neighboring eigenvalues of the Hamiltonian (2) in units of the corresponding mean level spacing Δ . We take pairs of energies close to the center of the spectrum including 60% of the spectrum. In Fig. 2 b we display the result for the model (2) at quarter filling and $t = U$, i. e. in phase I. The form of $P(s)$ is consistent with RMT-expectations, i.e. the Wigner-Dyson distribution of the Gaussian unitary ensemble, [7, 8]

$$P_{\text{GUE}}(s) = \frac{32}{\pi^2} s^2 e^{-\frac{4}{\pi} s^2}. \quad (4)$$

We thus observe a clear signature of quantum chaotic dynamics; the system under investigation is not integrable at $t = U$. For integrable phases, such as IV and IV', an absence of level repulsion is expected reflecting in the Poisson statistics $P_P(s) = e^{-s}$, see Fig. 2 a, c.

The RMT-behavior observed in phase I is consistent with findings in the SYK model (1) – away from half filling. [34] Our model (2) complies with this trend towards the Wigner-Dyson limit, Eq. (4) suggesting that phase I and the SYK-phase are adiabatically connected.

Level spacing ratios $r(s)$. In order to map out the phase boundaries, we employ the level spacing ratios [8,

35], defined as the

$$r_l = \frac{\min(s_l, s_{l+1})}{\max(s_l, s_{l+1})}. \quad (5)$$

The double average of r_l first over all pairs (s_l, s_{l+1}) per sample and second over the ensemble of samples defines the parameter \bar{r} , which is capable of distinguishing, e.g., different RMT-ensembles, as well as Poissonian level statistics. The latter corresponds to a value of $\bar{r} \approx 0.38$, while GUE statistics implies $\bar{r} \approx 0.599$ [8, 35, 36].

We determine the ratio \bar{r} in the parameter regime $10^{-3} \lesssim t/U \lesssim 200$, see Fig. 3.

Two transitions are seen, which separate the Poissonian boundary phases at $t=0$ (IV') and $U=0$ (IV) from a non-integrable region in between.

The transition near $U=0$ into IV is similar to the quadratic complex SYK model studied in Refs. [37, 38]. Integrability of the randomized all-to-all hopping at $U=0$ has an expression in terms of a large $SU(2)$ symmetry group, which tends to destroy level correlations. [37, 38]

In order to gather further evidence for identifying the chaotic phase seen in Fig. 3 with the SYK-phase embodied in Eq. (1), we extend the analysis of the level spacing ratios. We define a family of Hamiltonians that interpolates between the two models, Eq. (1) and (2), with a parameter $\lambda \in [0, 1]$:

$$\hat{H}(\lambda) = \lambda \cdot \hat{H}_{\text{cSYK}} + (1 - \lambda) \cdot \hat{H}_{tU}. \quad (6)$$

The level spacing ratios will, in general, depend on the family parameter, $\bar{r}(\lambda)$, taking a critical value, which differs from the RMT-value, if a phase-transition is crossed.

The inset of Fig. 3 displays the ratio $\bar{r}(\lambda)$ all along the line in parameter space connecting Hamiltonian (1)

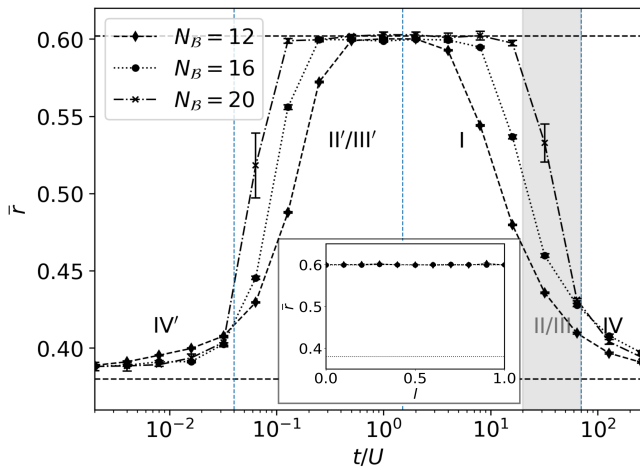


FIG. 3. Phase transition between localized (Poisson-type) and delocalized (Wigner-Dyson-type) level statistics. The dashed lines indicate Poissonian versus GUE behavior. [36] The nomenclature I, II/III and IV follows Ref. [30]; the labeling II'/III' and IV' is a generalization emphasizing the analogy. The different nature of the subphases I and II/III is not resolved with $\bar{r}(\lambda)$. Inset: Adiabatic connection of the level spacing statistics between Eq. (1) and (2), setting $U = t = J = 1$ with 5000/200/5 disorder realizations for $N_B = 12, 16, 20$.

at $\lambda=1$ to Hamiltonian (2) at $\lambda=0$. As is seen, the ratio is insensitive to λ , i.e., there is no indication of a phase transition - at least away from half filling and within the "range of visibility" of $\bar{r}(\lambda)$. The result strengthens the case that the chaotic phase of model (2) can indeed be identified with the non-Fermi-liquid phase of the SYK model.

Spectral form factor. Also the spectral form factor, $K(T)$, discriminates different phases from each other - and, as it turns out - with a sensitivity superior to $P(s)$ and $\bar{r}(\lambda)$; formally,

$$K(T) = \overline{|Z(\beta + iT)|^2}, \quad (7)$$

where $Z(\beta + iT)$ is the partition function taken at (inverse) temperature β and observation time T . The form factor $K(T)$ can be interpreted as a Fourier transformed correlator between energy levels. It is an established alternative descriptor of the level statistics and, hence, quantum chaos. In our simulations we focus on infinite temperature to probe homogeneously the entire spectrum. [39, 40] Then, a linear "ramp"-type feature characteristic of quantum chaotic systems is expected to appear in $K(T)$; it reveals itself in Fig. 4 at times $TJ \gtrsim \mathcal{O}(100)$, e.g., in phase I and it also emerges in the SYK model proper. [40–42]

We calculate the spectral form factor for different relative interaction strengths t, U such that the bandwidth fits the the SYK band width set by J in Eq. (1). Therefore, the energy scales of the two models as well as the

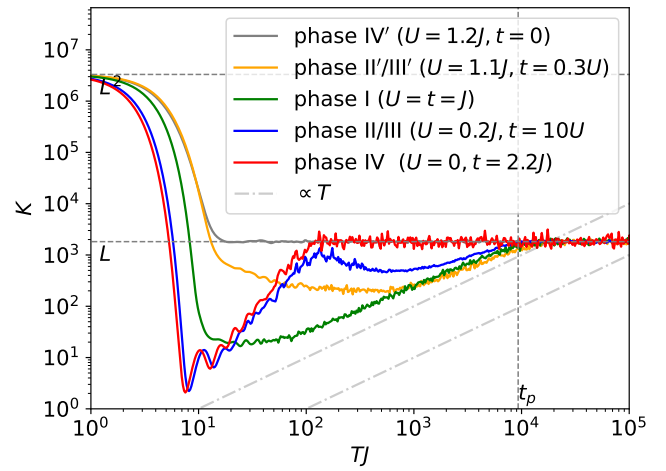


FIG. 4. Spectral form factor with its shape characteristic for the different phases IV', II'/III', I, II/III and IV. The dashed line indicates the behavior $K(T) \propto T$ as is appropriate for the RMT-type behavior also observed within SYK. Within region IV ($U=0$) we see a growth stronger than T . With our system sizes, the exponential behavior expected for integrable systems cannot be resolved. [37, 38] (Parameters: $N_B = 16$, 1000 disorder realizations, $t_p = 5L/J$)

different parameter settings of Eq. (2) can be directly compared. In the case of the quadratic model, phase IV ($U=0$), an exponential type of ramp has been reported for $K(T)$, based on analytical arguments and a numerical study. [37, 38] In Figs. 4 we confirm a ramp with very strong growth, e.g. in $TJ \gtrsim \mathcal{O}(100)$ for phases II/III and IV, increasing significantly faster than linear in T . In our model, Eq. (2), the exponential growth cannot be identified, however, in the hopping-dominated regime at $U=0$, i.e. in region IV - at least not within the system sizes at our disposal.

Interestingly, the purely interacting model, i.e. region IV' ($t=0$), does not exhibit a ramp-like behavior, even though it is integrable as is region IV. Thus in contrast to the level spacing ratio $P(s)$, the form factor $K(T)$ distinguishes the two integrable phases, IV and IV', from each other.

This finding is consistent with Prakash *et al.* [43], where above the localization transition triggered by a disordered Fock space diagonal term with completely uncorrelated energies, the linear ramp of an originally chaotic Hamiltonian vanishes.

In region I ($t \approx U$) we see in Fig. 4 an approximately linear ramp consistent with SYK and expectations from RMT and quantum chaos. In agreement with the SYK and RMT results the plateau assumes of $L = \binom{N_B}{N_B/4}$ - the number of energy levels - at the time $t_p \sim L/J$.

We note as a net outcome of this section that the model (2) has a structure in phase space substantially richer as compared to the SYK-model proper, (1). While this structure does not reveal in the simplest descriptors of the level statistics, i.e. $P(s)$ and $\bar{r}(\lambda)$, it becomes mani-

fest in the spectral form factor $K(T)$.

We add two remarks on further research that our observations could motivate. (a) The regions II/III and II'/III' exhibit their own individual and complex characteristics in the spectral form factor $K(T)$. Our preliminary data indicates a strong evolution of the shape of $K(T)$, seen in Fig. 4 in an intermediate time regime between $10 \lesssim TJ \lesssim 1000$. The detailed nature of this regime requires further studies.

(b) An interesting extension of the analysis of $K(T)$ concerns the low-temperature regime, $J\beta \gg 1$. Indeed, studies of other SYK-derived Hamiltonians that also have been equipped with a 1-body hopping term have indicated the possibility for a cross-over from a chaotic, incoherent metal regime at $\beta = 0$ to a (renormalized) Fermi liquid that occurs at low-enough temperatures. [26, 44] The finite temperature behavior of our model (2) has not been investigated yet and warrants a separate investigation. It will be interesting to see if also in our model (2) the high-temperature non-FL phase crosses over to a quasi-particle dominated regime at lowest temperatures.

B. Wave function statistics

The substructures I and II/III of the chaotic region have been analyzed before by Micklitz *et al.* [30] and Monteiro *et al.* [31]. For identification these authors employed the inverse participation ratio (IPR), which - for a given Fock-space basis - discriminates between localized states and also extended states with a different degree of delocalization. [31] The formal definition reads

$$I_q = \sum_{\nu} \overline{|\langle \nu | \Psi \rangle|^{2q}} \quad (8)$$

where the sum is over the Fock-space basis $|\nu\rangle$, see Sect. II. [45] Here, the overline indicates a double average over eigenvectors $|\Psi\rangle$ from the bulk of the spectrum of a given many-body Hamiltonian and over the disorder ensemble. Trivially, for completely localized wave functions we have $I_q = 1$ while for delocalized ones we will obtain the Porter-Thomas (PT) distribution

$$I_q = q! \mathcal{V}^{1-q}, \quad (9)$$

where $\mathcal{V} = \binom{N_B}{N_B/4}$ denotes the Fock space volume. Eq. (9) indicates that the statistics of wave-function components resembles independently distributed Gaussian variables.

In Fig. 5 we depict our computational result for I_2 and model (2). When averaging only wave functions from the center of the spectrum, i.e. the central fifth of the energy levels, have been included. We observe several qualitatively different regimes.

Region IV'. In the absence of hopping ($t=0$) wave-functions are localized in our chosen Fock-basis reflecting the fact that the interaction is of the density-density type

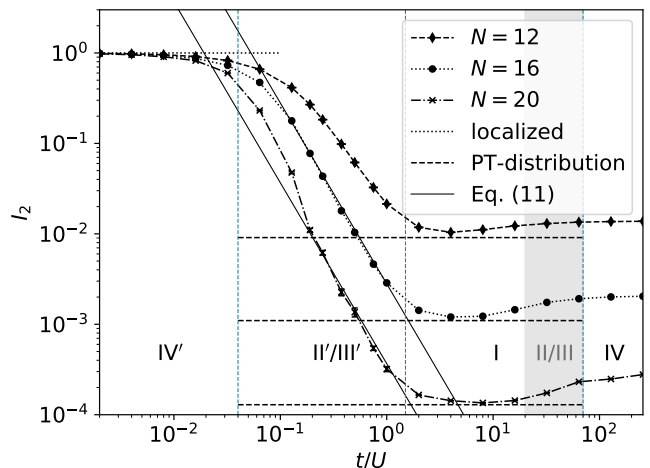


FIG. 5. Inverse participation ratio $I_2(t/U)$ for the phase diagram Fig. 2 at $\lambda = 0$ and system sizes $N_B = 12, 16, 20$. The dashed lines indicate genuine RMT behavior for a given systems size.^a Solid line indicates the NEE predictions, Eq. (10), with the constant $c = 0.5$. (Parameters: disorder average is performed over 5000/200/5 samples for $N_B = 12, 16, 20$ realizations.)

^a Baselines have been obtained by diagonalizing random unitary hermitian matrices of appropriate size.

and therefore diagonal in the basis chosen; $I_2 \approx 1$, correspondingly. The finding is consistent with integrability and our previous results derived from the level statistics.

Region I. In this regime, $t \gtrsim U$, RMT holds and the IPR approaches the Porter-Thomas result, Eq. (9), with increasing system size N_B .

Region IV. The model is integrable also in the non-interacting limit $U=0$. However, unlike it is the case with IV', the localized character of wavefunctions in Fock space does not reveal with the IPR in Fig. 5 due to the choice of our basis. For resolving this behavior the proper choice of basis is given by the eigenstates of t_{ij} in Eq. (2).

Region II/III. Refs. [30, 31] suggest that there is an intermediate phase (with two subphases II and III) that exhibits extended states, which do not fill all of the available Fock space (“non-ergodic”). In this non-ergodic extended (NEE) phase the level spacing statistics $P(s)$ is of the random matrix type. However in contrast to phase I, I_2 does not accept the Porter-Thomas form independent of t/U in II/III, in the limit of large N_B . As was already the case with IV, our choice of basis does not allow us to reveal this feature in Fig. 5.

Region II'/III'. However, in our model there is a dual phase II'/III', which separates the phase I from a second integrable point IV'. While the form-factor shows that this point is not to be identified with IV, it nevertheless allows for intermediate phases II'/III' analogous to II/III with IV. Instead, the IPR $I_2(t/U)$ is seen in Fig. 5 to exhibit a strong variation with its argument. It is a manifestation of the fact that wave functions occupy a small but non-zero fraction of the Hilbert space; they

are neither localized nor do they fully spread within the entire Fock space.

In Refs. [30, 31] the IPR $I_2(t/U)$ is predicted to follow a power law, $I_2(t/U) \propto (t/U)^a$; the exponent a is integer, either $a=1$ (in III) or $a=2$ (in II).[31] Our data confirms to this expectation with respect to III and $a=2$, see Fig. 5. The phase II with $a=1$ we do not resolve here, possibly due to restrictions in the available system size. For further analysis we adopt a formula derived analytically in [31]. It predicts the inverse participation ratio to follow a power-law

$$I_2 = c \cdot 8\sqrt{N_B} \frac{U^2}{\pi t^2 \binom{N_B}{N_B/4}}. \quad (10)$$

While the parametric scaling is expected to carry over also to our model, the prefactor c is left unspecified; Fig. 4 suggests $c \approx 0.5$.

C. Green's function

The RMT-phase I of model (2) is of central interest, because it may connect to the strong-coupling phase of the SYK model (1). We here continue our investigation of the phase I to provide further evidence supporting this adiabatic connectivity. Indeed, we already have demonstrated that the model (2) reproduces the characteristic statistical properties of the SYK model (1) in the chaotic phase and also the detailed structure of subphases that appear in SYK-derivatives. [30, 31] We now show that the models (1) and (2) may indeed share the characteristic power law structure of the Green's function, $G(i\omega) \propto \omega^{1/2}$ reflecting the conformal symmetry [1, 6], which is expected to hold in the frequency window

$$\frac{J}{N_B} \ll \omega \ll J. \quad (11)$$

Formally, the imaginary frequency Green's function is defined as the Fourier transform of

$$G(\tau) = G_i(\tau) = \langle [c_i^\dagger(\tau), c_i(0)] \rangle, \quad (12)$$

where the expectation value is taken over the ground state, we have a Lehmann representation

$$G(i\omega) = \sum_n \frac{\langle 0 | c_i | n \rangle \langle n | c_i^\dagger | 0 \rangle}{i\omega + E_0 - E_n} + \frac{\langle 0 | c_i^\dagger | n \rangle \langle n | c_i | 0 \rangle}{i\omega - E_0 + E_n}. \quad (13)$$

Here, $|n\rangle$ labels the exact eigenstates of the Hamiltonian and E_n the corresponding eigenenergies. $|0\rangle$ is the groundstate. We evaluate (13) by exact diagonalization of the Hamiltonians (1) and (2). The result is depicted in Fig. 6. As one might have expected, within the relevant frequency window the shape of $G(i\omega)$ as obtained for (2) is indeed roughly consistent with the SYK result (1). In both cases, the critical window of frequencies is

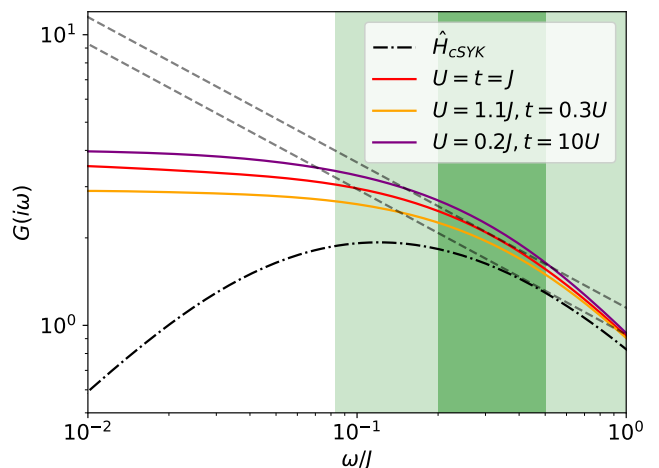


FIG. 6. Matsubara-Green's function of the model (2) for $N_B = 12$. The lightly shaded area, $J/N_B < \omega < J$, indicates the conformal window, (11); the dashed line represents the corresponding power law scaling $G(\omega) \propto \omega^{-1/2}$ scaling. Parameter settings of Hamiltonian (2) have been rescaled to ensure comparability between the respective models.

two narrow, however, in order to clearly identify a power law. That finite size effects could indeed be significant is seen from the fact that the scaling observed in the neighboring phases II/III and II'/III' is similar to the one seen in I. Since these phases are not of the RMT-type proper, a scaling with $\omega^{1/2}$ is not necessarily expected, here.

IV. SUMMARY AND CONCLUSION

Inspired by the SYK-model we have defined a fermionic Hamiltonian with a one body term and a density-density type interaction, both fully randomized. Our conceptual motivation was to investigate the phase diagram of the model, which is interesting in the broader context of many-body localization: it exhibits a rich structure allowing for two integrable and several chaotic phases, the latter being either ergodic or non-ergodic with respect to wavefunction spreading in Fock-space. Our practical motivation was that as compared to the SYK-model, our model is closer to microscopic realism in the sense that its interaction is of the density-density type. It therefore might help for identifying condensed-matter systems that exhibit phenomena to be interpreted in the SYK context.

The findings of our computational analysis summarize as follows: (i) Our model exhibits two integrable points. While both exhibit a Poissonian level spacing statistic, they exhibit markedly different spectral form factors. (ii) We find an RMT-type central phase that we argue to be adiabatically connected with the RMT-phase of the original model. In particular, we observe a conformal scaling $G(\omega) \propto \omega^{-1/2}$ of the Green's function - at least within the numerical limitations of our study. (iii) Similar to an SYK-derived model studied in Refs. [30, 31], our model

also exhibits intermediate phases with RMT-type level spacing statistics and extended, but non-ergodic wavefunctions. In this regime the scaling of the IPR with the model parameters is quadratic, $(t/U)^2$, consistent with what was found numerically and analytically in Ref. [31]. Summarizing, the model we propose represents a significant step from the SYK-model towards microscopic realism. It exhibits a phase diagram much richer as compared to SYK, but it still keeps a central phase that appears to exhibit all key features of SYK-physics.

We conclude by putting our work into perspective with other studies from the recent literature; table I offers a brief account of relevant works. A variety of disorder models has been studied limiting the range of interactions down to power-law envelopes for the kinetic (exponent α) and interaction (exponent β) terms. They constitute links in an evolutionary chain born at the SYK model proper (1) and its variations in Tab. I, top section, and then connecting via our model Eq. (2) followed by those listed in Tab. I, bottom section, to physical realism. How the corresponding phase diagram will evolve as moving along this chain is an interesting question, which here we have to leave to future research.

References	model	α, β	\tilde{t}_{ij}	\tilde{U}_{ij}	ϵ_i
Ref. [1, 6]	majorana	$\alpha, \beta=0$	0	SYK	nr
Ref. [5, 46]	fermion	$\alpha, \beta=0$	0	SYK	nr
Ref. [8, 9, 15, 31]	majorana	$\alpha, \beta=0$	r	SYK	nr
This work	fermion	$\alpha, \beta=0$	r	r	nr
Ref. [47]	spin	$\alpha, \beta \in (d, 3)$	r	r	r
Ref. [48]	spin	$\alpha=\beta \in (d, 2d)$	r	r	r
Ref. [49]	fermion	$\alpha, \beta \in (0, 2.5)$	r	r	r
Ref. [50]	fermion	$\alpha \in (1, 4), \beta=\infty$	r	nr	r
Ref. [51]	fermion	$\alpha=\beta \in (0.5, 3)$	nr	nr	r
Ref. [52]	spin	$\alpha=\beta \in (0.5, 2.5)$	nr	nr	r
Ref. [53]	spin	$\alpha=\beta \in (1.75, \infty)$	nr	nr	r
Ref. [54]	fermion	$\alpha \in (1.2, 4), \beta=\infty$	nr	nr	r
Ref. [55]	spin	$\alpha, \beta \in (0, \infty)$	nr	nr	r
Ref. [56]	boson	$\alpha, \beta \in (0, \infty)$	nr	nr	r

TABLE I. Literature survey on models connecting to our model Eq. (2) including fermion, boson and spin types. Disorder may enter in a hopping term, $t_{ij}=\tilde{t}_{ij}/|i-j|^\alpha$, with randomized amplitude \tilde{t}_{ij} and in a similarly randomized two-body density interaction, $U_{ij}=\tilde{U}_{ij}/|i-j|^\beta$, and as randomized on-site potentials, ϵ_i . In [52, 56] power-law correlated disorder has been implanted into t_{ij}, U_{ij} by randomizing the site locations. Abbreviations: r for randomized and nr for non-randomized; $\beta=\infty$ indicates nearest-neighbor interactions; SYK denotes an interaction as in Eq. (1), i.e. deviating from the density-density form.

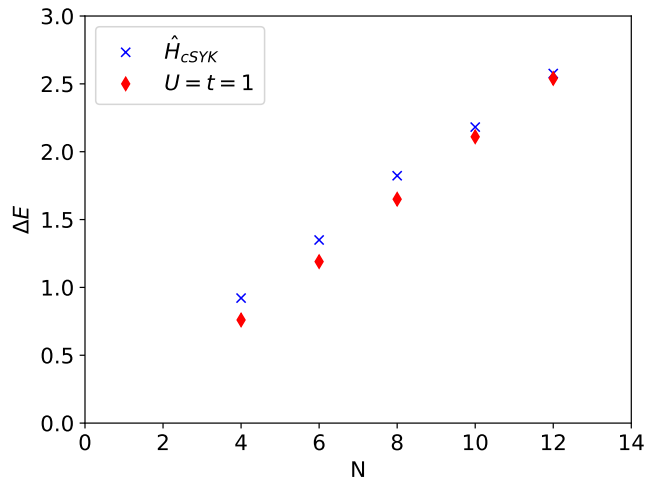


FIG. 7. Extensive scaling of the bandwidth of the SYK model (1) and Hamiltonian (2). We calculate ΔE for different system sizes N_B . The bandwidth is averaged over 1000 disorder realizations for $N_B = 4, 6$ and 100 realizations for $N_B = 8, 10, 12$.

ACKNOWLEDGEMENTS

FE thanks Alexander Altland for an inspiring conversation that has partially initiated this work. JD thanks Torsten Weber for insightful discussions. JD and FE acknowledge fruitful discussions on computational aspects with Christoph Lehner. SB received support from SERB-DST, India, through Ramanujan Fellowship (No. SB/S2/RJN-128/2016), Early Career Research Award (No. ECR/2018/000876), Matrics (No. MTR/2019/000566), and MPG for funding through the Max Planck Partner Group at IITB. Support from German Research Foundation (DFG) through the Collaborative Research Center, Project ID 314695032 SFB 1277 (projects A03, B01) and through EV30/11-1, EV30/12-1 and EV30/14-1 are acknowledged.

Appendix A: Normalizing energy scale

In order to quantitatively compare results for the Hamiltonian models (1) (parameter J) and (2) (parameters t, U), we here determine the energy normalization. We focus on the example $t = U$. The full bandwidth of the many-body problem $\Delta E = E_{max} - E_{min}$ scales extensively, see Fig. 7, thus the normalization scale $\epsilon = \Delta E/N_B$ is intensive. In order to compare the low frequency properties of the Green's function with the SYK model, we calculate the quantity ϵ for the SYK model and scale the Hamiltonian (2) so as to give the same value. For instance, in the case depicted in Fig. 7 we obtain $\epsilon \approx 0.22J$.

- [1] J. Maldacena and D. Stanford, *Physical Review D* **94**, 106002 (2016).
- [2] A. Kitaev and S. J. Suh, *Journal of High Energy Physics* **2018**, 1 (2018).
- [3] A. M. García-García and J. J. Verbaarschot, *Physical Review D* **94**, 126010 (2016).
- [4] J. Polchinski and V. Rosenhaus, *Journal of High Energy Physics* **2016**, 1 (2016).
- [5] Y. Gu, A. Kitaev, S. Sachdev, and G. Tarnopolsky, *Journal of High Energy Physics* **2020**, 1 (2020).
- [6] A. Kitaev, University of California, Santa Barbara USA **7** (2015).
- [7] J. Behrends and B. Béri, *Physical Review D* **101**, 066017 (2020).
- [8] A. M. García-García, B. Loureiro, A. Romero-Bermúdez, and M. Tezuka, *Physical review letters* **120**, 241603 (2018).
- [9] M. Haque and P. A. McClarty, *Physical Review B* **100**, 115122 (2019).
- [10] B. Kobrin, Z. Yang, G. D. Kahanamoku-Meyer, C. T. Olund, J. E. Moore, D. Stanford, and N. Y. Yao, arXiv preprint arXiv:2002.05725 (2020).
- [11] A. M. García-García and J. J. Verbaarschot, *Physical Review D* **96**, 066012 (2017).
- [12] For example, at generic choices of N_B and μ the symmetry class is Gaussian unitary, but at special points it also can be GSE or GOE; e.g. a half filled sector at $N_B = 12$ has GOE statistics. [3, 7].
- [13] J. Maldacena, S. H. Shenker, and D. Stanford, *Journal of High Energy Physics* **2016**, 106 (2016).
- [14] J. Maldacena, *International journal of theoretical physics* **38**, 1113 (1999).
- [15] A. Lunkin, K. Tikhonov, and M. Feigel'man, *Physical Review Letters* **121**, 236601 (2018).
- [16] A. Altland, D. Bagrets, and A. Kamenev, *Physical Review Letters* **123**, 106601 (2019).
- [17] S. Banerjee and E. Altman, *Physical Review B* **95**, 134302 (2017).
- [18] A. Altland, D. Bagrets, and A. Kamenev, *Physical Review Letters* **123**, 226801 (2019).
- [19] C. Proust and L. Taillefer, *Annual Review of Condensed Matter Physics* **10**, 409 (2019).
- [20] A. Legros, S. Benhabib, W. Tabis, F. Laliberté, M. Dion, M. Lizaire, B. Vignolle, D. Vignolles, H. Raffy, Z. Li, *et al.*, *Nature Physics* **15**, 142 (2019).
- [21] C. M. Varma, arXiv preprint arXiv:1908.05686 (2019).
- [22] S. Sachdev, *Quantum phase transitions* (Wiley Online Library, 2007).
- [23] D. Van Der Marel, H. Molegraaf, J. Zaanen, Z. Nussinov, F. Carbone, A. Damascelli, H. Eisaki, M. Greven, P. Kes, and M. Li, *Nature* **425**, 271 (2003).
- [24] A. A. Patel and S. Sachdev, *Physical review letters* **123**, 066601 (2019).
- [25] A. Altland, D. Bagrets, and A. Kamenev, *Physical Review Letters* **123**, 226801 (2019).
- [26] O. Parcollet and A. Georges, *Physical Review B* **59**, 5341 (1999).
- [27] P. Cha, N. Wentzell, O. Parcollet, A. Georges, and E.-A. Kim, *Proceedings of the National Academy of Sciences* **117**, 18341 (2020).
- [28] H. Guo, Y. Gu, and S. Sachdev, *Physical Review B* **100**, 045140 (2019).
- [29] D. Chowdhury, Y. Werman, E. Berg, and T. Senthil, *Physical Review X* **8**, 031024 (2018).
- [30] T. Micklitz, F. Monteiro, and A. Altland, *Physical review letters* **123**, 125701 (2019).
- [31] F. Monteiro, T. Micklitz, M. Tezuka, and A. Altland, *Physical Review Research* **3**, 013023 (2021).
- [32] Technically, the Hamiltonian can be rewritten in spin basis by means of the Jordan-Wigner transformation
- $$c_i^\dagger = \left[\prod_{j=1}^{i-1} \sigma_j^z \right] \sigma_i^+, \quad (\text{A1})$$
- where $\sigma_i^\pm = 1/2(\sigma_i^x \pm i\sigma_i^y)$ and $\sigma_i^{x,y,z}$ the Pauli-matrices in x, y, z direction at site i [46, 57]. With this transformation the Hamiltonian (2) is rewritten in matrix form and can be diagonalized numerically.
- [33] Our code development is building on an early version employed in Ref. Rossini *et al.* [58]. The interface is written in python, while the Hamiltonian matrix and the Green's function routine employ Fortran. The computation time at $N = 20$ on one core takes ≈ 3 hours per disorder realization at a quarter filling.
- [34] Strictly speaking, RMT-statistics is expected only in the limit of large system sizes. However, as indicated by our data in Fig. 2 the asymptotics can be detected for this class of models already at relatively moderate system sizes.
- [35] E. Cuevas, M. Feigel'Man, L. Ioffe, and M. Mezard, *Nature communications* **3**, 1 (2012).
- [36] Y. Atas, E. Bogomolny, O. Giraud, and G. Roux, *Physical review letters* **110**, 084101 (2013).
- [37] Y. Liao, A. Vikram, and V. Galitski, arXiv preprint arXiv:2005.08991 (2020).
- [38] M. Winer, S.-K. Jian, and B. Swingle, *Physical Review Letters* **125**, 250602 (2020).
- [39] E. Brézin and S. Hikami, *Physical Review E* **55**, 4067 (1997).
- [40] J. S. Cotler, G. Gur-Ari, M. Hanada, J. Polchinski, P. Saad, S. H. Shenker, D. Stanford, A. Streicher, and M. Tezuka, *Journal of High Energy Physics* **2017**, 118 (2017).
- [41] A. Altland and D. Bagrets, *Nuclear Physics B* **930**, 45 (2018).
- [42] P. Saad, S. H. Shenker, and D. Stanford, arXiv preprint arXiv:1806.06840 (2018).
- [43] A. Prakash, J. Pixley, and M. Kulkarni, arXiv preprint arXiv:2008.07547 (2020).
- [44] X.-Y. Song, C.-M. Jian, and L. Balents, *Phys. Rev. Lett.* **119**, 216601 (2017).
- [45] We here adopt the nomenclature I_q for the IPR rather than the more conventional P_q so as to avoid confusion with the level-spacing statistics $P(s)$.
- [46] W. Fu and S. Sachdev, *Physical Review B* **94**, 035135 (2016).
- [47] A. L. Burin, *Phys. Rev. B* **91**, 094202 (2015).
- [48] K. S. Tikhonov and A. D. Mirlin, *Phys. Rev. B* **97**, 214205 (2018).
- [49] S. J. Thomson and M. Schiró, *Phys. Rev. Research* **2**, 043368 (2020).

- [50] G. De Tomasi, *Phys. Rev. B* **99**, 054204 (2019).
- [51] S. Nag and A. Garg, *Phys. Rev. B* **99**, 224203 (2019).
- [52] A. Safavi-Naini, M. L. Wall, O. L. Acevedo, A. M. Rey, and R. M. Nandkishore, *Phys. Rev. A* **99**, 033610 (2019).
- [53] B. Kloss and Y. Bar Lev, *Phys. Rev. B* **102**, 060201 (2020).
- [54] R. Modak and T. Nag, *Phys. Rev. E* **101**, 052108 (2020).
- [55] S. Roy and D. E. Logan, *SciPost Phys.* **7**, 42 (2019).
- [56] X. Deng, G. Masella, G. Pupillo, and L. Santos, *Phys. Rev. Lett.* **125**, 010401 (2020).
- [57] L. García-Álvarez, I. Egusquiza, L. Lamata, A. Del Campo, J. Sonner, and E. Solano, *Physical review letters* **119**, 040501 (2017).
- [58] D. Rossini, G. M. Andolina, D. Rosa, M. Carrega, and M. Polini, *Physical Review Letters* **125**, 236402 (2020).